Study of isolated prompt photon production in p-Pb collisions for the ALICE kinematics

Muhammad Goharipour[*] and Hossein Mehraban[†]

Faculty of Physics, Semnan University, Semnan P.O. Box 35131- 19111, Semnan, Iran
(Received 19 January 2017; published 3 March 2017)

Prompt photon production is known as a powerful tool for testing perturbative QCD predictions and also the validity of parton densities in the nucleon and nuclei, especially of the gluon. In this work, we have performed a detailed study on this subject, focusing on the isolated prompt photon production in p-Pb collisions at forward rapidity at the LHC. The impact of input nuclear modifications obtained from different global analyses by various groups on several quantities has been investigated to estimate the order of magnitude of the difference between their predictions. We have also studied in detail the theoretical uncertainties in the results due to various sources. We found that there is a remarkable difference between the predictions from the nCTEQ15 and other groups in all ranges of photon transverse momentum p_T^γ. Their differences become more explicit in the calculation of the nuclear modification ratio and also the yield asymmetry between the forward and backward rapidities rather than single differential cross sections. We emphasize that future measurements with ALICE will be very useful, not only for decreasing the uncertainty of the gluon nuclear modification, but also to accurately determine its central values, especially in the shadowing region.

I. INTRODUCTION

It is well known that the large momentum transfer processes play an important role in testing perturbative quantum chromodynamics (pQCD) because the asymptotic freedom property allows us to apply the perturbative techniques to make predictions for processes that are dominated by short-distance interactions. In hadronic collisions, since photons couple in a pointlike fashion to the quark constituents of the colliding hadrons, they provide an excellent probe for such purposes [1–5]. The study of prompt photons (photons not originating from meson decays) is also very useful to obtain direct information on the parton distribution functions (PDFs), especially for the gluon [6–10]. Moreover, it has been established that prompt photon production in association with a heavy quark (either charm or bottom) can be used for searching the intrinsic heavy quark components of the nucleon [11,12].

In heavy-ion collisions, the production of photons is recognized as an important tool [13] to study the fundamental properties of deconfined, strongly interacting matter, namely, the quark gluon plasma (QGP) [14,15] created in these collisions. Actually, photons can provide information on the whole time evolution and dynamics of the medium because they are not accompanied by any final-state interaction. For example, measuring their transverse momentum distribution can be used to estimate the temperature of the system. It is worth noting that, in nucleus-nucleus collisions, direct photons come from a variety of different sources and can be divided into two categories: thermal photons that have a thermal origin and prompt photons coming from cold processes. Usually, prompt photons are considered as a background to thermal photons when we are looking for signals of the QGP. Thermal photons dominate the direct photon spectrum at low photon transverse momentum p_T^γ, while prompt photons are the dominant photon source at high p_T^γ. Although in heavy-ion collisions there is no straightforward way to distinguish between thermal and prompt photons experimentally, the fact that different processes are dominant at different p_T^γ can help us to unfold the different contributions to the total observed yields.

The measurement of direct photons in heavy-ion collisions has been performed so far in many experiments [16–25]. For gold-gold collisions, one can refer, for example, to the PHENIX Collaboration measurements at center-of-mass energy of $\sqrt{s} = 200$ GeV, where the photons have the transverse momentum $1 \lesssim p_T \lesssim 20$ GeV [17,18]. The ALICE Collaboration has reported the first measurement of a low-p_T direct photon at the LHC from lead-lead collisions at $\sqrt{s} = 2.76$ TeV [24,25]. Such measurements have also been done by PHENIX in Au-Au collisions at the RHIC [19,20]. The measurement of prompt photon production at the LHC has also been performed by the ATLAS [22] and CMS [23] Collaborations in lead-lead collisions at $\sqrt{s} = 2.76$ TeV in the ranges $22 < p_T < 280$ GeV and $20 < p_T < 80$ GeV, respectively. Note that in these kinematic regions, photons are expected to be dominantly produced in hard partonic collisions. For the case of d-Au collisions, we only have the PHENIX measurement at $\sqrt{s} = 200$ GeV [26].

*m.goharipour@semnan.ac.ir
†hmehraban@semnan.ac.ir

Despite all of these experimental efforts, there is still no measurement of direct photon production in p-A collisions, though the ALICE measurement in p-Pb collisions will be reported in the near future [27].

In order to calculate cross sections in any nuclear collision, one needs to know the structure of the colliding nuclei. This structure can be described by nuclear parton distribution functions (NPDFs), similar to the PDFs in the case of hadron structure. The required nuclear parton densities can be extracted using the nuclear experimental data and Dokshitzer-Gribove-Lipatov-Alterelli-Parisi (DGLAP) evolution equations within the collinear factorization [28,29]. However, NPDFs cannot be well determined using the available nuclear deep inelastic scattering (DIS) and Drell-Yan experimental data compared to the free nucleon PDFs. Consequently, the obtained NPDFs from different global analyses by various groups [30–38] have some considerable differences, both in behavior and uncertainty. This can lead to different results for predictions of physical observables that are sensitive to NPDFs. Since in nuclear collisions prompt photons are produced in hard scatterings of incoming partons, they can provide some information on parton densities in nuclei, especially for the gluon PDF [39–43]. In this work, we investigate the impact of various recent NPDFs and their uncertainties on the theoretical predictions of isolated prompt photon production in p-Pb collisions at the LHC. More emphasis will be placed on the recent nCTEQ15 NPDFs.

The present paper is organized as follows. In Sec. II, we discuss the gluon density of the proton and its nuclear modification for the Pb nucleus and compare the predictions of various phenomenological groups at different factorization scales. In Sec. III, we briefly describe the physics of prompt photon production. We pay particular attention to its main concepts such as involved leading order (LO) and next-to-leading order (NLO) subprocesses, direct and fragmentation components of the cross section, and the definition of isolation cut. The isolated prompt photon production in pp and p-Pb collisions at forward rapidity at the LHC is studied in Sec. IV. The differential cross sections are calculated as functions of p_T^γ using various modern PDF and NPDF sets to estimate the order of magnitude of the difference between their predictions. Section V is devoted to studying the theoretical uncertainties in the differential cross section of isolated prompt photon production due to various sources. In Sec. VI, we calculate and compare the nuclear modification ratio $R_{p\text{-Pb}}^\gamma$ and the yield asymmetry between the forward and backward rapidities $Y_{p\text{-Pb}}^{\text{asym}}$ using different nuclear modifications. Finally, we summarize our results and conclusions in Sec. VII.

II. GLUON DENSITY OF THE PROTON AND ITS NUCLEAR MODIFICATIONS

The accurate determination of PDFs is crucial for all calculations of high-energy processes with initial hadrons,

whether within the standard model (SM) or when exploring new physics. It is well known that the PDFs are non-perturbative objects, and one needs to extract them from the global fits to hard-scattering data. The reason for this is that they cannot be determined from the first principles of QCD, although their scale dependence is determined by the perturbative DGLAP evolution equations. Nowadays, global analyses of PDFs are performed using a large number of available precise experimental data from the DIS, Drell-Yan, and collider experiments, and our knowledge of the quark and gluon substructure of the nucleon has been improved to a large extent. Consequently, the extracted PDFs by different analyst groups [44–51] are satisfactorily accurate and also in a good agreement with each other. However, there are still some variations in both their central values and uncertainties, especially in the case of gluon and sea quarks. Therefore, the study of those observables that are sensitive enough to the specific parton distributions and can distinguish between them is of utmost importance both experimentally and theoretically.

Since in this work we study isolated direct photon production at LHC energies, the gluon density is our first choice (see next section). Figure 1 shows a comparison between the gluon distributions from the recent well-known phenomenological groups, namely, CT14 [45], MMHT14 [46], and NNPDF3.0 [47]. We have plotted their NLO results in terms of the Bjorken scaling variable x at two low (top panel) and high (bottom panel) scales $Q^2 = 2$ and 100 GeV^2. The comparison has been made as the ratio to CT14 (as a reference PDF set) including PDF uncertainties to make the differences between the results more clear. As can be seen, the predictions of these groups for the gluon distribution differ significantly in some values of x. Most differences occur in the small and large x regions. Regardless of these regions, it may be of interest that the NNPDF3.0 has a significant enhancement at x of about 0.1. Another conclusion that can be drawn from Fig. 1 is that the gluon distribution from the CT14 has a greater uncertainty (blue band) than the MMHT14 (red band) and NNPDF3.0 (green band) in all values of x.

In contrast to the PDFs, the results obtained for the NPDFs are not very satisfying due to the lack of experimental data. In fact, since the current NPDF analyses [30–38] are mainly constrained by DIS and Drell-Yan data, only the quark nuclear modifications at fairly large values of x can be controlled as well. Although the nuclear gluon distributions can be constrained indirectly via DGLAP evolution at higher orders of perturbation theory, we know that it is not enough for making accurate theoretical predictions of physical observables that are sensitive to the gluon density. In this way, some phenomenological groups have used the inclusive pion production data from d-Au collisions at RHIC in addition to the DIS and Drell-Yan data. Very recently, Eskola *et al.* [37] have also used the LHC proton-lead data in their analysis. However, due to
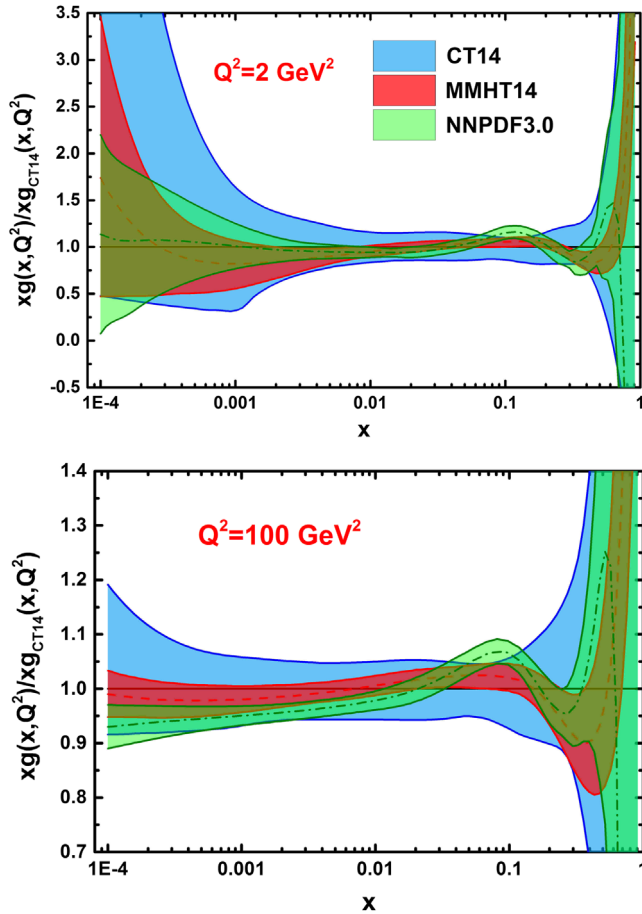
FIG. 1. Ratio of the NLO gluon distributions with their uncertainties from various PDF sets: CT14 [45] (blue band), MMHT14 [46] (red band), and NNPDF3.0 [47] (green band) to the CT14 central value at two scales $Q^2 = 2$ (top panel) and 100 (bottom panel) GeV^2.

the limited kinematic reach of data, the gluon modifications and also their uncertainties obtained by various groups are very different in almost all values of x. It should be noted that, at the moment, there is only one analysis including the LHC p-Pb data.

There are different approaches for determining the bound-proton PDFs. Usually, they are defined in terms of nuclear modifications R_i^A. To be more precise, R_i^A are the scale-dependent ratios between the PDF of a proton inside a nucleus, $f_i^{p/A}$, and that in the free proton, f_i^p,

$$R_i^A(x, Q^2) \equiv \frac{f_i^{p/A}(x, Q^2)}{f_i^p(x, Q^2)}. \quad (1)$$

This approach has been used in the EPS09 [32], DSSZ [33], HKN07 [34], KA15 [35], and EPPS16 [37] analyses. Note that, in this method, the extracted nuclear modifications are dependent on the chosen PDFs of the free proton. For example, the HKN07 and EPS09 NPDFs are based on the MRST1998 free-proton [52] and CTEQ6.1M [53] sets,

respectively. However, there is another approach used by the nCTEQ group [30,31] in which the NPDF parametrizations do not rely on a factorization into a nuclear modification factor and free-proton PDFs. Actually, in this approach, the NPDFs are parametrized directly as a function of x at the starting scale Q_0^2, and then an explicit A dependence is introduced in the coefficients of their functional form. It should be mentioned here that to obtain bound-neutron PDFs, one must assume the isospin symmetry. So, for the average up (u) and down (d) quark PDFs in a nucleus A with Z protons, we have

$$u_A(x, Q^2) = \frac{Z}{A} R_u^A f_u^p + \frac{A - Z}{A} R_d^A f_d^p,$$

$$d_A(x, Q^2) = \frac{Z}{A} R_d^A f_d^p + \frac{A - Z}{A} R_u^A f_u^p. \quad (2)$$

The nuclear modifications, Eq. (1) can be divided into four areas as a function of x: (1) a suppression for $x \lesssim 0.01$ that is commonly referred to as shadowing; (2) an antishadowing area in which R_i^A has an enhancement around $x \sim 0.1$; (3) the European Muon Collaboration (EMC) effect, a depletion at $0.3 \lesssim x \lesssim 0.7$; and finally, (4) a Fermi motion region in which R_i^A again undergoes an excess towards $x \to 1$. Figure 2 shows a comparison between the nuclear modifications of the gluon PDF in a Pb-nucleus with their uncertainties from the nCTEQ15 [31] (blue band), EPS09 [32] (red band), DSSZ [33] (green band), and HKN07 [34] (pink band) at $Q^2 = 2$ (top panel) and 100 (bottom panel) GeV^2. One can clearly see that there are remarkable differences between their central values and uncertainties almost in all the ranges of x. Among them, the nCTEQ15 shows stronger shadowing, antishadowing, and EMC effect. Moreover, its prediction has a wider error band than other groups in all values of x. The EPS09 has a similar treatment to nCTEQ15 but somewhat milder and also with less uncertainty. Although the DSSZ does not show the shadowing in small values of x at $Q^2 = 2$ GeV^2, it appears in higher values of Q^2 due to the evolution effects. Nevertheless, the gluon shadowing in DSSZ is very small, just like the antishadowing, EMC effect, and Fermi motion, so the DSSZ prediction for the gluon nuclear modification of the lead nucleus stays around 1 in all regions. Another interesting point that can be gained from Fig. 2 is that the HKN07 does not show the EMC effect for low or high Q^2 values. In conclusion, one can expect that these differences lead to the different results for predictions of physical observables that are sensitive to the gluon density and thus the gluon nuclear modification. Note that for the LHC with high values of center-of-mass energy $\sqrt{s}$, depending on the transverse momentum p_T and pseudorapidity η of photons, various x regions can be explored in the target and the projectile. Actually, with the naive LO $2 \to 2$ kinematics, the momentum fractions typically probed by direct photon production are
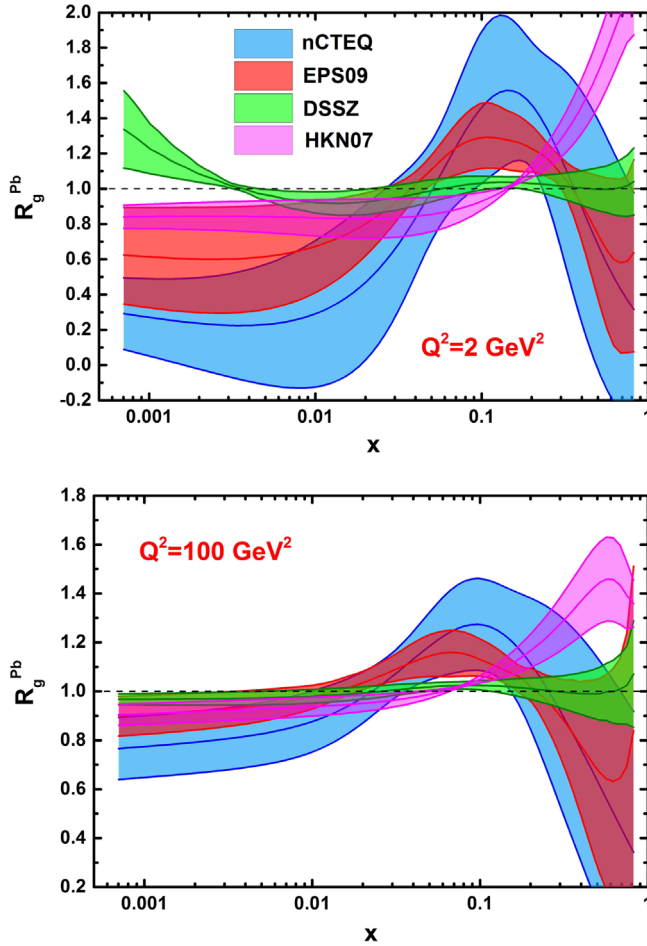
FIG. 2.   A comparison between the nuclear modifications of the gluon PDF in a Pb-nucleus with uncertainties from the nCTEQ15 [31] (blue band), EPS09 [32] (red band), DSSZ [33] (green band), and HKN07 [34] (pink band) at $Q^2 = 2$ (top panel) and 100 (bottom panel) GeV^2.

$$x_{1,2} \approx \frac{2p_{\mathrm{T}}}{\sqrt{s}} e^{\pm \eta}. \tag{3}$$

Therefore, for a given $\sqrt{s}$ and p_{T}, and for the case in which η increases, the process becomes sensitive to parton densities at smaller x_2 (target) and larger x_1 (projectile). In the next section, we briefly review the physics of the prompt photon production in the LHC collisions as an excellent probe for the gluon distribution of the proton and its corresponding nuclear modification.

III. PHYSICS OF PROMPT PHOTON PRODUCTION

For more than three decades, many studies have been done on the prompt photon production [1–5,54–74]. In this section, we briefly discuss the prompt photon physics and related topics. By definition, "prompt photons" are those photons that arise from processes during the collision and are not produced from the decay of hadrons, such as π_0, η,

etc. produced at large transverse momenta. Forward prompt photons consist of two types of photons: direct and fragmentation photons. Direct photons that behave as high-p_{T} colorless partons are produced predominantly from the initial hard scattering processes of the colliding quarks or gluons. Fragmentation photons behave as a kind of hadron; i.e., they are produced as bremsstrahlung emitted by a scattered parton, from the fragmentation of high-p_{T} quarks, and as gluons which are produced in primary hard partonic collisions or from the interaction of a scattered parton with the medium created in heavy-ion collisions [75,76]. Although the direct and fragmentation components of the prompt photon cross section described above cannot be measured separately in the experiments, the theoretical calculations can be performed completely separately. In this way, the cross section for the inclusive prompt photon production in a collision of hadrons h_1 and h_2 can be written generally as follows:

$$d\sigma_{h_1 h_2}^{\gamma + X} = d\sigma_{h_1 h_2}^{\mathrm{D}\gamma + X} + d\sigma_{h_1 h_2}^{\mathrm{F}\gamma + X}, \tag{4}$$

where D and F refer to the direct and fragmentation parts, respectively, and X indicates the inclusive nature of the cross section. On the other hand, using collinear factorization [28,29], the cross section for the inclusive production of a hard elementary particle k in $h_1 h_2$ collisions can be calculated as

$$d\sigma_{h_1 h_2}^{k+X} = \sum_{i,j} f_i^{h_1}(x_1, M^2) \otimes f_j^{h_2}(x_2, M^2)$$
$$\otimes d\hat{\sigma}_{i,j}^{k+X'}(\mu^2, M^2, M_F^2), \tag{5}$$

where $f_i^{h_1}(x_1, M^2)$ and $f_j^{h_2}(x_2, M^2)$ are the PDFs of parton species i and j inside the projectile (h_1) and target (h_2), respectively, at momentum fractions x_1 and x_2 and factorization scale M of the initial-state parton distributions. In the above equation, $\otimes$ is a convolution integral over x_1 and x_2. Moreover, the partonic pieces $d\hat{\sigma}_{i,j}^{k+X'}$ denoted by M, renormalization scale μ, and factorization scale M_F of the photon fragmentation function (FF) can be calculated as a perturbative expansion in the strong (α_s) and electroweak (α) couplings. (Note that the partonic pieces $d\hat{\sigma}_{i,j}^{k+X'}$ do not have any dependence on the factorization scale M_F in the Born approximation. However, such dependence appears in the calculation of the higher-order corrections to both the direct and fragmentation components from which final-state collinear singularities have been subtracted according to the $\overline{\mathrm{MS}}$ factorization scheme [62].) As usual, X' indicates that in the calculation of $d\hat{\sigma}_{i,j}^{k+X'}$, we must integrate over everything but the photon. Then, we can calculate the direct component of the prompt photon production cross section in Eq. (4) using Eq. (5) and assuming particle k as a photon γ.

The experimentally measured prompt photons also include the fragmentation photons emitted through collinear fragmentation of a parton that is itself produced with a large transverse momentum. The fragmentation component of the prompt photon production cross section in Eq. (1) can be calculated as follows:

$$d\sigma_{h_1 h_2}^{\mathrm{F}\gamma + X} = \sum_{i,j,k} f_i^{h_1}(x_1, M^2) \otimes f_j^{h_2}(x_2, M^2)$$
$$\otimes \, d\hat{\sigma}_{i,j}^{k+X'}(\mu^2, M^2, M_F^2) \otimes D_{\gamma/k}(z, M_F^2). \quad (6)$$

In this equation, $D_{\gamma/k}(z, M_F^2)$ is the parton-to-photon FF, where z is the fractional momentum over which the last convolution is taken. Actually, in the calculation of the fragmentation contribution, occurrence of some singularities, including a final-state quark-photon collinear singularity or final-state multiple collinear singularities at higher orders, is inevitable. These singularities are resummed and absorbed into FFs of the photons. In this case, since the fragmentation functions behave roughly as $\alpha/\alpha_s(M_F^2)$ [1,2], the perturbatively calculable pieces related to the partonic subprocesses, $d\hat{\sigma}_{i,j}^{k+X'}$, can be of the order of α_s^2 for LO and α_s^3 for NLO parton production. Consequently, the fragmentation contributions of the cross section remain of the same order as the direct contributions.

Now we are in a position to introduce all partonic subprocesses that contribute to the prompt photon production cross section at LO and NLO approximation. At LO, there are two Born-level subprocesses: the Compton scattering $q(\bar{q})g \to \gamma q(\bar{q})$ and annihilation $q\bar{q} \to \gamma g$. The importance of these subprocesses clearly depends on the type of collisions. Actually, in pp collisions at RHIC and LHC, the $q\bar{q}$ annihilation channel has a small contribution to the cross sections in all kinematic regions, whereas at the Tevatron, this channel is also considerable. At NLO, there are more contributing subprocesses, including $q(\bar{q})g \to \gamma g q(\bar{q})$, $q\bar{q} \to \gamma gg$, and other subprocesses from the virtual corrections to the Born-level processes. It is worth pointing out in this context that since at the LHC the $q\bar{q}$ annihilation is suppressed compared to other subprocesses, and on the other hand, the gluon distribution is dominant rather than the sea quark distributions at small x, the prompt photon production provides direct information on the proton gluon distribution. It should also be taken into account that because of the high center-of-mass energy, the photon production at the LHC probes values of x that are considerably smaller than at the Tevatron.

In order to reject the background of photons coming from the decays of hadrons such as π_0, η produced in the collision that are not considered prompt photons by definition, an isolation criterion is required. Various isolation criteria have been used so far in related studies [62,77–79]. The most common criterion which can also be implementable at the partonic level is the cone criterion [62]. According to the cone isolation criterion, a photon is considered an isolated photon if, in a cone of radius R in rapidity y and azimuthal angle ϕ around the photon direction,

$$(y - y_\gamma)^2 + (\phi - \phi_\gamma)^2 \leq R^2, \quad (7)$$

the amount of accompanying hadronic transverse energy $E_{\mathrm{T}}^{\mathrm{had}}$ is smaller than some finite value $E_{\mathrm{T\,max}}$,

$$E_{\mathrm{T}}^{\mathrm{had}} \leq E_{\mathrm{T\,max}}. \quad (8)$$

Both R and $E_{\mathrm{T\,max}}$ are chosen by the experiment, and $E_{\mathrm{T\,max}}$ is presented as a fixed value or a fixed fraction of the transverse momentum of the photon p_{T}^γ or, more generally, as a function of p_{T}^γ.

One of the main differences between the direct and fragmentation photons is that a direct photon will most probably be separated from the hadronic environment, whereas a fragmentation photon, except for the case in which the photon carries away most of the momentum of the fragmenting parton, is most probably accompanied by hadrons. In this way, since the isolation cut discards the prompt photon events that have too much hadronic activity around the photon, and on the other hand, the fragmentation photons are emitted collinearly to the parent parton, it is expected that the isolation cut reduces the fragmentation component. Now, considering what was said above, in the next section, we calculate and study in detail the prompt photon production in pp and p-Pb collisions at center-of-mass energy of 8.8 TeV and for the forward rapidities corresponding to the ALICE kinematics [27].

IV. STUDY OF ISOLATED PROMPT PHOTON PRODUCTION AT ALICE

The LHC allows us to investigate the behavior of SM particles in a qualitatively new energy region via measuring the production of various particles such as the W and Z bosons in association with jets [80] or a heavy flavor quark [81,82] and also the isolated prompt photon, whether inclusively [83–87] or in association with jets [88,89]. In the previous section, we presented main topics related to the prompt photon production in hadron collisions. In this section, we present theoretical predictions for the isolated prompt photon production in pp and p-Pb collisions at $\sqrt{s} = 8.8$ TeV corresponding to the ALICE kinematics [27]. All calculations are performed here, and subsequent sections are based on the JETPHOX Monte Carlo program [5,62,63], which includes both direct and fragmentation processes and also allows us to study the isolation cut. We include all diagrams up to LO and NLO of QED and QCD coupling, respectively, defined in the $\overline{\mathrm{MS}}$ renormalization scheme. Within the JETPHOX framework, it is also possible to compute direct and fragmentation parts as distinct; however, the NLO calculations are performed at the parton level and do not
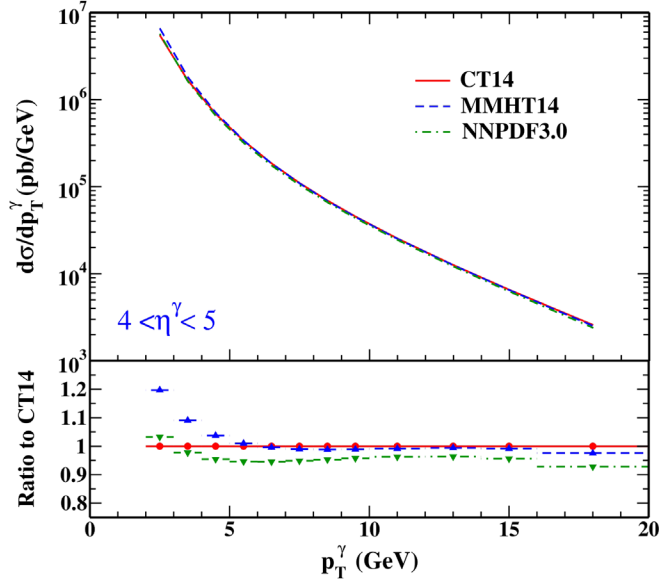
FIG. 3.   A comparison of the NLO theoretical predictions for the differential cross section of isolated prompt photon production in pp collisions as a function of p_T^γ using three various NLO PDFs of CT14 [45] (red solid), MMHT14 [46] (blue dashed), and NNPDF3.0 [47] (green dotted-dashed) at $\sqrt{s} = 8.8$ TeV for $4 < \eta^\gamma < 5$. The ratios of the results to the CT14 prediction have been shown in the bottom panel.
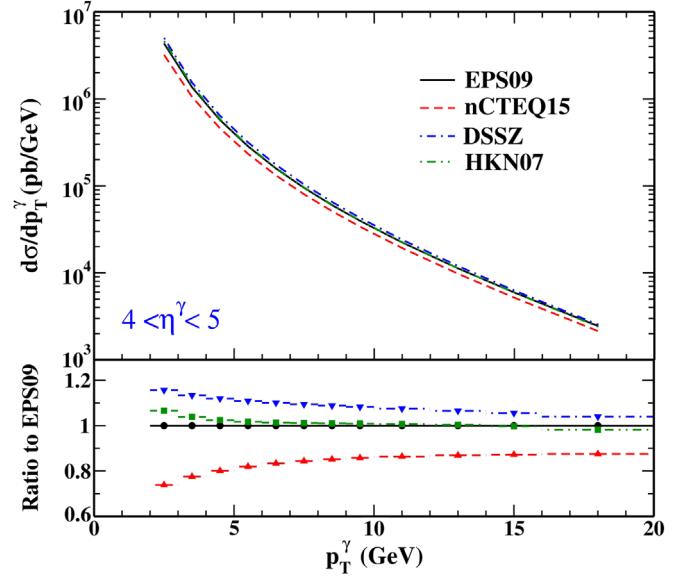
FIG. 4.   A comparison of the NLO theoretical predictions for the differential cross section of isolated prompt photon production in p-Pb collisions as a function of p_T^γ using the EPS09 [32] (black solid), nCTEQ15 [31] (red dashed), DSSZ [33] (blue dotted-dashed), and HKN07 [34] (green dotted-dotted-dashed) nuclear modifications and the CT14 free-proton PDFs [45] at $\sqrt{s} = 8.8$ TeV for $4 < \eta^\gamma < 5$. The ratios of the results to the EPS09 prediction are shown in the bottom panel.

account for hadronization effects. It should be noted that, in our numerical calculations performed in this section and also Sec. VI, we use set II of the NLO Bourhis-Fontannaz-Guillet (BFG) FFs of photons [90] for calculating the fragmentation component of the cross sections [Eq. (6)]. Moreover, the renormalization (μ), factorization (M), and fragmentation (M_F) scales are set to the photon transverse momentum ($\mu = M = M_F = p_T^\gamma$). The FFs and scale uncertainties are studied separately in the next section, in addition to the theoretical uncertainties due to NPDFs. As a last point, note that the fine-structure constant (α_{EM}) is set to the JETPHOX default of $1/137$.

Now we are in a position to calculate the isolated prompt photon production in pp collisions at $\sqrt{s} = 8.8$ TeV theoretically, using various modern PDF sets, CT14 [45], MMHT14 [46], and NNPDF3.0 [47], introduced in Sec. II. In this way, we can estimate the variation of the results due to the different PDF sets. Note that for each group, the NLO PDF sets with $\alpha_s(M_Z) = 0.118$ are taken by virtue of the LHAPDF package [91]. Figure 3 shows the differential cross sections obtained as a function of p_T^γ in the kinematic range $2 < p_T^\gamma < 20$ GeV for the forward region $4 < \eta^\gamma < 5$. We should note that in calculating the cross sections, we have used a tighter isolation cut, $E_T^{had} < 2$, with $R = 0.4$ [see Eqs. (7) and (8)]. As can be seen, all predictions are in good agreement with each other almost in all regions of p_T^γ. However, in order to investigate in more detail the differences between the predictions in various

regions of p_T^γ, we have plotted their ratios to the CT14 prediction in the bottom panel of Fig. 3. The only significant difference occurs at $p_T \simeq 2$, where the MMHT14 prediction differs from the CT14 and NNPDF3.0 ones up to 20%. Besides this, we can state that the differences between them are less than 10% in all values of p_T^γ.

In Sec. II, we have shown that the nuclear modifications of the gluon distribution from various phenomenological groups differ from each other, to a large extent, almost in all values of x. Now, as a next step, we calculate the NLO differential cross section of the isolated prompt photon production in p-Pb collisions at $\sqrt{s} = 8.8$ TeV in order to study the impact of input nuclear modifications on the final results and estimate the order of magnitude of the difference between their predictions. To this end, we take the nuclear modifications, Eq. (1), from the nCTEQ15 [31], EPS09 [32], DSSZ [33], and HKN07 [34] and choose the CT14 PDF sets for the free-proton PDFs. The calculations are performed again for the forward region $4 < \eta^\gamma < 5$. The results obtained have been compared in Fig. 4 as a function of p_T^γ in the kinematic range of $2 < p_T^\gamma < 20$ GeV. In the bottom panel, we have shown their ratios to the EPS09 prediction. As a result, one can clearly see that these groups have different predictions for isolated prompt photon production at the ALICE kinematics. Although the HKN07 is in a good agreement with EPS09 in all values of p_T^γ, the DSSZ and nCTEQ15 have significant deviations, especially at smaller values of p_T^γ. Overall, the nCTEQ15 which presented the

newest modern NPDFs (among the sets considered in this work) has the greatest difference from the others, and its prediction is placed below them. Note that according to Eq. (3), for the p-Pb collisions and kinematics used here, the photon probes the NPDFs in small values of x_2 corresponding to the shadowing region in Fig. 2. Then, due to the large differences observed in Fig. 4, measurements of isolated prompt photon production at the ALICE kinematics can be really helpful in constraining the gluon nuclear modifications and determining their best central values in the shadowing region. The differences between the various gluon modifications from different groups can be made more explicit if one calculates the minimum bias nuclear modification ratio for p-Pb collisions and also the yield asymmetry between the forward and backward rapidities. We study these quantities separately in Sec. VI. In the next section, we investigate the theoretical uncertainties in the differential cross section of isolated prompt photon production due to NPDF, scale, and FF uncertainties.

V. STUDY OF THEORETICAL UNCERTAINTIES

In the previous section, we calculated the cross section of isolated prompt photon production in p-Pb collisions using various nuclear modifications of PDFs for the Pb nucleus. Now, it is important and also interesting to calculate the theoretical uncertainties in the results with respect to the various sources. The most important sources of uncertainties are the PDF, NPDF, scale, and FF uncertainties. Since the theoretical uncertainties of the free-proton PDFs have been studied before in many papers concerning the isolated prompt photon production in pp collisions, and on the other hand, since we are interested here in p-Pb collisions and thus the impact of NPDFs on the cross section, we ignore the study of PDF uncertainties (note, however, that PDFs have smaller uncertainties than NPDFs).

To study the NPDF uncertainties, we choose the nuclear modifications from the nCTEQ15 [31] as our baseline, which has greatest uncertainties in comparison with other groups according to Fig. 2. The theoretical uncertainties of nuclear modifications can be obtained as usual using the 32 error sets of the nCTEQ15 parametrization, as shown in Fig. 2 by the blue band. For calculating such uncertainties to any physical quantity related to NPDFs such as the isolated prompt photon production considered here, one must vary the error sets and calculate the deviations from the central result (the best-fit value) and then the contribution to the size of the upper and lower errors via

$$\delta^+ X = \sqrt{\sum_i [\max(X_i^{(+)} - X_0, X_i^{(-)} - X_0, 0)]^2},$$

$$\delta^- X = \sqrt{\sum_i [\max(X_0 - X_i^{(+)}, X_0 - X_i^{(-)}, 0)]^2}. \quad (9)$$

The other important sources of theatrical uncertainties in the cross section of isolated prompt photon production are the uncertainties due to the scale variations. As mentioned, we have set the renormalization, factorization, and fragmentation scales as $\mu = M = M_F = p_T^\gamma$ in all calculations performed in the previous section. Although no optimal scale choice is possible for the prediction of the inclusive photon cross section in the region of phase space of interest [92], it is expected that the predictions can be reliably made by this choice. Moreover, we expect that the theoretical uncertainty due to scale variations can be calculated by changing these scales by a factor 2 and comparing the $2p_T^\gamma$ and $\frac{1}{2} p_T^\gamma$ results. However, the more correct method in the calculation of scale uncertainties is the combination of both incoherent and coherent scale variations. In this method, an incoherent variation means varying the scales independently by a factor of 2 around the central value so that one scale is varied while keeping the other two equal to p_T^γ, and a coherent variation means varying the scales simultaneously by a factor of 2 around the central value as before. Finally, we can calculate the total scale uncertainty by adding in quadrature all obtained uncertainties.

Since, as mentioned in Sec. III, prompt photon production consists of both direct and fragmentation contributions, it is inevitably related to the FFs that appeared in the fragmentation component [see Eq. (6)]. Then, the part of the theoretical uncertainties in its cross section comes from the FF uncertainties. Unfortunately, at present, because of the lack of experimental data for inclusive photon production in $e^+ e^-$ annihilation as a best source to constrain the photon fragmentation functions, our knowledge about them, especially for the case of gluon fragmentation to photons, is not satisfactory. Note that, for example, the ALEPH and HRS data on ρ production have been used in the BFG parametrizations [90]. Consequently, their gluon fragmentation to photons has a large uncertainty and is parametrized with sets I and II. Although the significant difference between these two sets appears at low scales and may not matter at LHC energies, it is interesting to see to what extent the isolated prompt photon cross section is impacted by changing the FF set. In the previous section, the BFG set II was used to calculate the fragmentation component of the cross sections. In this section, we use set I to estimate the FF uncertainties by comparing the results with the previous ones.

Now, according to what was said above, we are ready to calculate the theoretical uncertainties in the cross section of isolated prompt photon production in p-Pb collisions at $\sqrt{s} = 8.8$ TeV due to the NPDF, scale, and FF uncertainties. Figure 5 shows the results obtained as a function of p_T^γ for the forward region $4 < \eta^\gamma < 5$ using the nCTEQ15 [31] parametrizations as inputs for the nuclear modifications. In this figure, the dotted curve represents the results obtained using the BFG set I for the FFs, and the red and blue bands represent the scale and NPDF uncertainties, respectively.
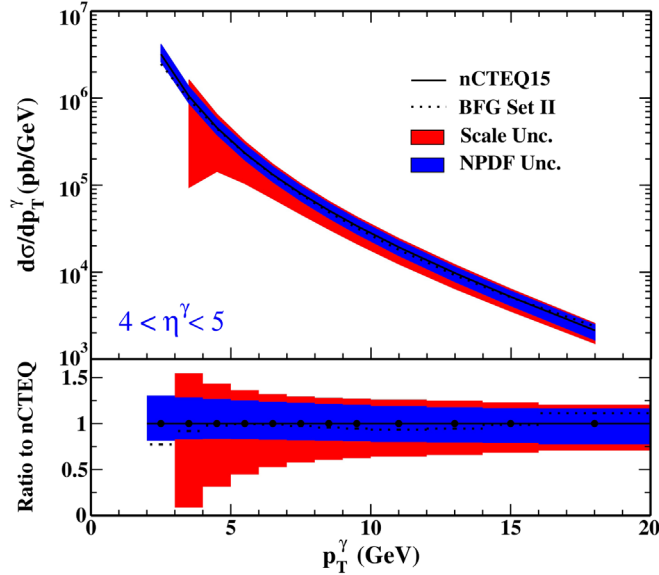
FIG. 5.   A comparison between the NPDF, scale, and FF uncertainties in the differential cross section of isolated prompt photon production in p-Pb collisions at $\sqrt{s} = 8.8$ TeV as a function of p_T^γ for the forward region $4 < \eta^\gamma < 5$. The black solid and dotted curves are the nCTEQ15 [31] predictions using FFs from the BFG sets II and I [90], respectively. The red band represents the scale uncertainties. The nCTEQ15 NPDF uncertainties are shown by the blue band. The bottom panel shows the ratios to the nCTEQ15 central prediction.

Note that the black solid curve corresponds to the results obtained in the previous section using the nCTEQ15 central set and also the BFG set II. As before, the ratios to the nCTEQ15 central prediction are shown in the bottom panel. As can be seen, there is not significant difference between the predictions obtained using the FFs of BFG sets I and II. Some deviations are seen just at low and large values of p_T^γ. The scale uncertainties are dominant rather than NPDF uncertainties in all the ranges of p_T^γ, and they become very large at low p_T^γ. Note that we have plotted the scale uncertainties for $p_T^\gamma > 3$ GeV because, for its smaller values, the cross section becomes unphysical when one sets the scales to the lower value $\mu = \frac{1}{2} p_T^\gamma$. It is also worth noting here that if one considers only the coherent scale variations to calculate the scale uncertainties, a narrow error band is obtained in almost all p_T^γ regions, so the scale uncertainties do not even exceed 5%.

VI. NUCLEAR MODIFICATION AND FORWARD-TO-BACKWARD RATIOS

In the previous section, we found that the theoretical uncertainties due to the scale variations can be very large, especially at low values of p_T^γ if one uses the method in which the combination of both incoherent and coherent scale variations is considered. On the other hand, there are also PDF and FF uncertainties besides the NPDF
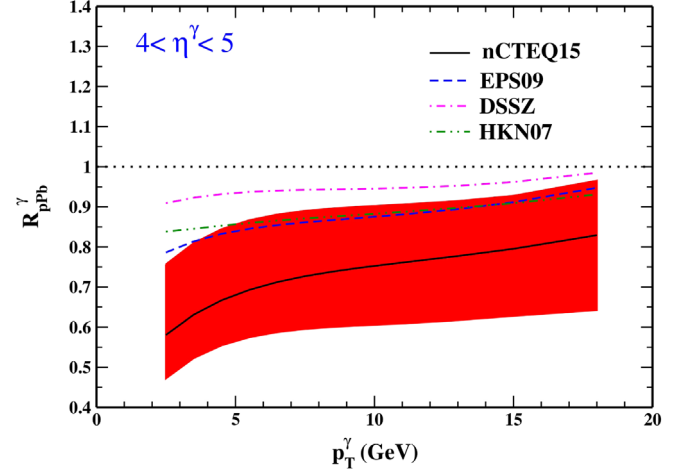

FIG. 6.   A comparison between the nuclear modification ratios $R_{p\text{-Pb}}^\gamma$ for p-Pb collisions at $\sqrt{s} = 8.8$ TeV and $4 < \eta^\gamma < 5$ using the nCTEQ15 [31] (black solid), EPS09 [32] (blue dashed), DSSZ [33] (pink dotted-dashed), and HKN07 [34] (green dotted-dotted-dashed) nuclear modifications and the CT14 free-proton PDFs [45]. The red band corresponds to the nCTEQ15 NPDF uncertainties.

uncertainties. In this way, it is very desirable to have a quantity that is not only more sensitive to the nuclear modifications, but also one in which the other sources of theoretical uncertainties are canceled to a large extent. In this regard, the minimum bias nuclear modification ratio is a good choice [43]. For the prompt photon production in p-Pb collisions at the LHC, it is defined as

$$R_{p\text{-Pb}}^\gamma \equiv \frac{d\sigma/dp_T(p + \text{Pb} \to \gamma + \text{X})}{208 \times d\sigma/dp_T(p + p \to \gamma + \text{X})}. \quad (10)$$

Note that because of the isospin effect, the nuclear modification ratio Eq. (10) is not normalized to 1 when no nuclear modifications in the parton densities are assumed. However, the isospin effect becomes more important whenever the valence quark sector of the nuclei is probed. The predictions for $R_{p\text{-Pb}}^\gamma$ at $4 < \eta^\gamma < 5$ and $\sqrt{s} = 8.8$ TeV are shown in Fig. 6 in the kinematic range $2 < p_T^\gamma < 20$ GeV. In this figure, the central nCTEQ15 [31] prediction has been shown as a black solid line, and the red band corresponds to its uncertainty range; the EPS09 [32], DSSZ [33], and HKN07 [34] predictions are represented by the blue dashed, pink dotted-dashed, and green dotted-dotted-dashed curves, respectively. It should be noted that for free-proton PDFs, whether in the numerator or the denominator of Eq. (10), we have again used the CT14 PDFs [45]. As can be seen, there is a remarkable difference between the nCTEQ15 prediction and other groups in all the ranges of p_T^γ. Note that the DSSZ prediction is not even within the large error band of the nCTEQ15. It indicates that future measurements with

ALICE will be very useful not only for decreasing the uncertainty of the gluon nuclear modification but also to accurately determine its central values in the shadowing region.

Although the nuclear modification ratio Eq. (10) is a quantity with a high sensitivity to the nuclear modifications in PDFs and is also largely indifferent to the PDF, FF, and scale uncertainties, we can define the other quantity that does not require a $p + p$ baseline measurement with the same $\sqrt{s}$. It is the yield asymmetry between the forward and backward rapidities, which for p-Pb collisions is defined as follows:

$$Y_{p\text{-Pb}}^{\text{asym}} \equiv \frac{d\sigma/dp_{\text{T}}(p + \text{Pb} \to \gamma + \text{X})|_{\eta \in [\eta_1, \eta_2]}}{d\sigma/dp_{\text{T}}(p + \text{Pb} \to \gamma + \text{X})|_{\eta \in [-\eta_2, -\eta_1]}}. \quad (11)$$

Such an observable has the advantage that it is free from the absolute normalization uncertainty included due to involving the Glauber modeling [93] for the cases in which the luminosity for the collected data sample is not measured. Also, some correlated systematic uncertainties can be expected to cancel.

According to Eq. (3), the isolated photon production at backward rapidities will be sensitive to the nuclear anti-shadowing and EMC effect of NPDFs. This means that in this kinematic region the nuclear valence quark modifications also become important since the sensitivity of the cross section to them is raised towards larger values of x_2. It is now interesting to calculate the differential cross sections and also nuclear modification ratios at backward rapidities before calculating the forward-to-backward ratios. Figure 7 shows the NLO theoretical predictions for the differential cross section of isolated prompt photon production as a function of p_{T}^γ using the EPS09 (black solid), nCTEQ15 (red dashed), DSSZ (blue dotted-dashed), and HKN07 (green dotted-dotted-dashed) nuclear modifications and CT14 free-proton PDFs at $\sqrt{s} = 8.8$ TeV for the backward region $-5 < \eta^\gamma < -4$. The ratios of the results to the EPS09 prediction have been shown in the bottom panel. In analogy to the forward region $4 < \eta^\gamma < 5$ (see Fig. 4), the differences between the predictions are smaller; thus, the DSSZ and HKN07 have a very similar behavior in all values of p_{T}^γ, and their predictions only have a little difference from the EPS09 prediction at low and high p_{T}^γ regions. Although the differences between the nCTEQ15 prediction and other groups are somewhat decreased in the backward region, there are still considerable deviations. Note also that unlike the forward case, the nCTEQ15 prediction is placed on the top of other predictions due to its larger nuclear antishadowing, and it becomes closer to them towards the EMC effect region.

The nuclear modification ratios $R_{p\text{-Pb}}^\gamma$ for p-Pb collisions at $\sqrt{s} = 8.8$ TeV and the backward region $-5 < \eta^\gamma < -4$ are shown in Fig. 8, where the black solid, blue dashed, pink dotted-dashed, and green dotted-dotted-dashed curves
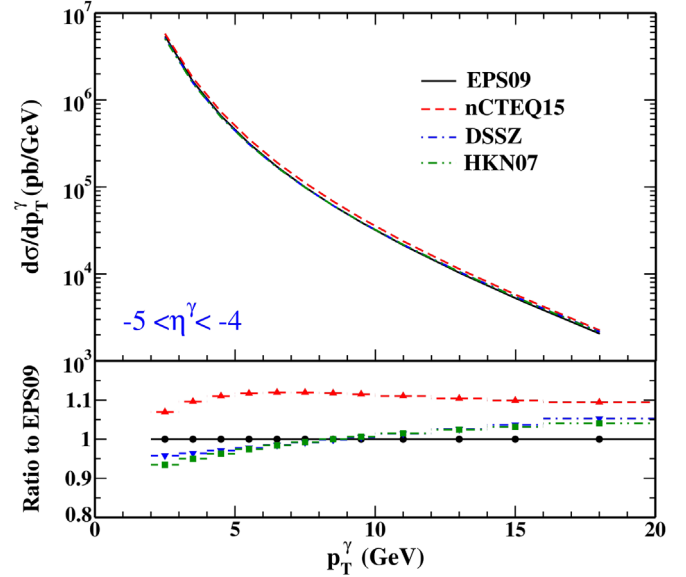

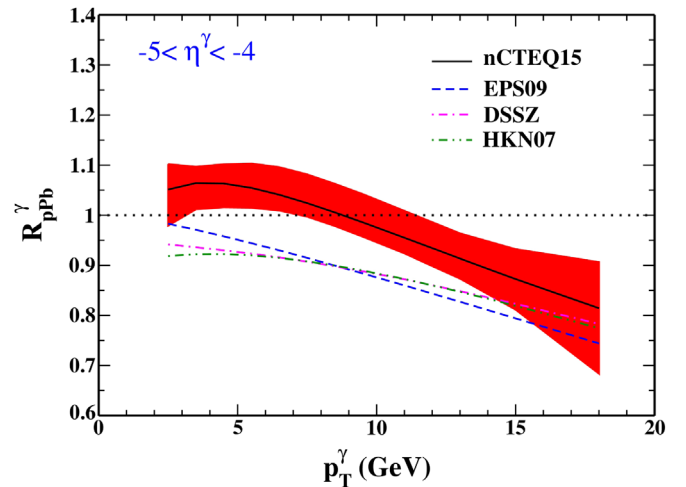FIG. 7. Same as Fig. 4, but for the backward region $-5 < \eta^\gamma < -4$.

FIG. 8. Same as Fig. 6, but for the backward region $-5 < \eta^\gamma < -4$.

correspond to the nCTEQ15, EPS09, DSSZ, and HKN07 predictions, respectively, and the free-proton PDFs have been taken again from the CT14. The red band corresponds to the nCTEQ15 NPDF uncertainties. As expected, the EPS09, DSSZ, and HKN07 predictions are in good agreement with each other, and nCTEQ15 has significant deviations from them. It should be noted that only the nCTEQ15 predicts a value greater than 1 for $R_{p\text{-Pb}}^\gamma$ in this kinematic region. Moreover, the NPDF error band of nCTEQ15 is clearly smaller than the corresponding band in the forward direction (see Fig. 6). This is due to the fact that the NPDFs are constrained better in the antishadowing and EMC effect regions than the shadowing with experimental data now available.
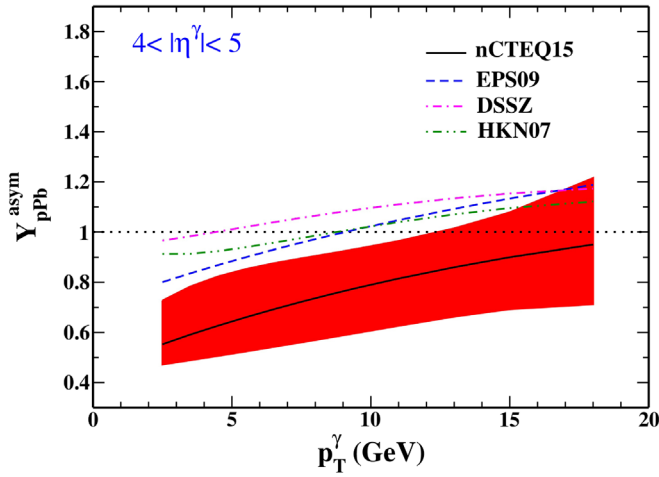
FIG. 9. A comparison between the forward-to-backward yield asymmetries $Y_{p\text{-Pb}}^{\text{asym}}$ for the isolated prompt photon production in p-Pb collisions at $\sqrt{s} = 8.8$ TeV and $4 < |\eta^\gamma| < 5$ using the nCTEQ15 [31] (black solid), EPS09 [32] (blue dashed), DSSZ [33] (pink dotted-dashed), and HKN07 [34] (green dotted-dotted-dashed) nuclear modifications and CT14 free-proton PDFs [45]. The red band corresponds to the nCTEQ15 NPDF uncertainties.

FIG. 10. A comparison between the nuclear modification ratios $R_{p\text{-Pb}}^\gamma$ as a function of η^γ for p-Pb collisions at $\sqrt{s} = 8.8$ TeV with $2 < p_T^\gamma < 20$ GeV using the nCTEQ15 [31] (black solid), EPS09 [32] (blue dashed), DSSZ [33] (pink dotted-dashed), and HKN07 [34] (green dotted-dotted-dashed) nuclear modifications and CT14 free-proton PDFs [45].

The corresponding results of the forward-to-backward yield asymmetries $Y_{p\text{-Pb}}^{\text{asym}}$ for the isolated prompt photon production in p-Pb collisions at $\sqrt{s} = 8.8$ TeV and $4 < |\eta^\gamma| < 5$ are shown in Fig. 9. The predictions have been made again using the nCTEQ15 (black solid), EPS09 (blue dashed), DSSZ (pink dotted-dashed), and HKN07 (green dotted-dotted-dashed) nuclear modifications and the CT14 free-proton PDFs. In comparison with the nuclear modification ratios (Fig. 6), the nCTEQ15 still has the greatest difference from the others, and its prediction is placed below them in all values of p_T^γ. It is interesting that in this case all three EPS09, DSSZ, and HKN07 predictions are not even within the error band of nCTEQ15. Note also that the nCTEQ15 does not reach 1 even at high values of p_T^γ, while the other groups predict a value greater than 1 for $Y_{p\text{-Pb}}^{\text{asym}}$ almost at $p_T^\gamma \gtrsim 9$ GeV. However, the NPDF error band of nCTEQ15 (red band) has not changed significantly except for the very low p_T^γ region. It is worth remembering that the yield asymmetries are sensitive to two very different x_2 regions. Nevertheless, overall, a partial cancellation of the uncertainties in $Y_{p\text{-Pb}}^{\text{asym}}$ occurs if the forward and backward nuclear modification ratios are sensitive to the same nuclear effect. Based on the results obtained in this section, one can simply conclude that in order to accurately determine the NPDFs and judgements about which one of them has more accurate behavior in various x regions, the measurements of $Y_{p\text{-Pb}}^{\text{asym}}$ are more preferred, especially if done with sufficient accuracy.

As a last step, to further explore the impact of input nuclear modifications on the cross section of isolated prompt photon production in p-Pb collisions, we calculate
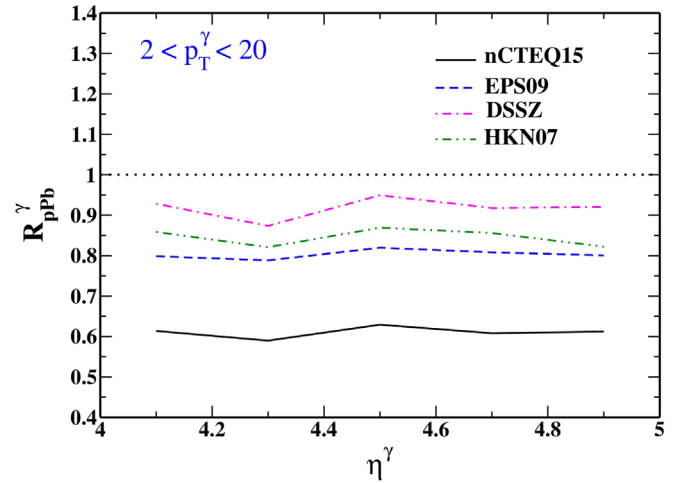
the nuclear modification ratios $R_{p\text{-Pb}}^\gamma$ as a function of photon pseudorapidity η^γ using various NPDFs and compare them with each other. Figure 10 shows the results obtained at $\sqrt{s} = 8.8$ TeV for $2 < p_T^\gamma < 20$ GeV and in the kinematic range $4 < \eta^\gamma < 5$. The nCTEQ15, EPS09, DSSZ, and HKN07 predictions are shown with the black solid, blue dashed, pink dotted-dashed, and green dotted-dotted-dashed curves, respectively. As can be seen, in analogy with Fig. 6, the differences between the predictions are a little clearer in this case. Therefore, the measurements of $R_{p\text{-Pb}}^\gamma$ as a function of η^γ can also be helpful in the determination of nuclear modifications.

VII. SUMMARY AND CONCLUSIONS

Photon production in hadron collisions is known as an important tool for testing perturbative QCD predictions. One of the main motivations of the study of prompt photon production is that it is very useful to obtain direct information on the gluon PDFs of both nucleons and nuclei. Since the NPDFs cannot be well determined using the available experimental data compared with the PDFs of free nucleon, the obtained NPDFs from different global analyses by various groups have some considerable differences both in behavior and uncertainty. This can lead to the different results for predictions of physical observables that are sensitive to NPDFs. In this work, we investigated the impact of various recent NPDFs on the theoretical predictions of isolated prompt photon production in p-Pb collisions at the LHC for the ALICE kinematics to estimate the order of magnitude of the difference between their predictions. We also studied in detail the theoretical uncertainties in the cross sections due

to the NPDF, scale, and FF uncertainties. We found that there is no significant difference between the predictions obtained using different FFs of BFG sets I and II in the ALICE kinematics. The scale uncertainties are dominant rather than the NPDF uncertainties in all the ranges of p_T^γ, and they become very large at low p_T^γ, if one uses the method in which the combination of both incoherent and coherent scale variations is considered. However, if one considers only the coherent scale variations, a narrow error band is obtained in almost all p_T^γ regions, so the scale uncertainties do not even exceed 5%. Moreover, we found that there is a remarkable difference between the predictions from the nCTEQ15 and other groups in all ranges of p_T^γ. Their differences become more explicit in the calculation of the nuclear modification ratio $R_{p\text{-Pb}}^\gamma$ and also in the yield asymmetry between the forward and backward rapidities $Y_{p\text{-Pb}}^{\text{asym}}$ rather than a single differential cross section. For the forward $R_{p\text{-Pb}}^\gamma$, the DSSZ prediction is not even within the large error band of nCTEQ15. Such a situation occurs for the backward $R_{p\text{-Pb}}^\gamma$ and also the yield asymmetries $Y_{p\text{-Pb}}^{\text{asym}}$ in almost all p_T^γ regions, but this time for all three EPS09, DSSZ, and HKN07 predictions. Overall, the NPDF error band of nCTEQ15 in the backward direction is smaller than the corresponding band in the forward direction. This is due to the fact that the isolated photon production at backward rapidities is sensitive to the nuclear antishadowing and EMC effect of NPDFs, which are constrained better than the shadowing with the experimental data now available. However, the NPDF error band of nCTEQ15 from $R_{p\text{-Pb}}^\gamma$ to $Y_{p\text{-Pb}}^{\text{asym}}$ has not changed significantly except for the very low p_T^γ region. Based on the results obtained, we concluded that in order to accurately determine the NPDFs and judgements about which one of them has more accurate behavior in various x regions, the measurements of $Y_{p\text{-Pb}}^{\text{asym}}$ are more preferred, especially if done with sufficient accuracy. In addition, the future measurements with ALICE will be very useful not only for decreasing the uncertainty of the gluon nuclear modification but also to accurately determine its central values, especially in the shadowing region. As further investigation, we calculated the nuclear modification ratio $R_{p\text{-Pb}}^\gamma$ as a function of photon pseudorapidity η^γ using various NPDFs. We found that the differences between the predictions are a little clearer in this case. It seems that the measurements of $R_{p\text{-Pb}}^\gamma$ as a function of η^γ can also be helpful in the determination of nuclear modifications.

ACKNOWLEDGMENTS

[1] P. Aurenche, A. Douiri, R. Baier, M. Fontannaz, and D. Schiff, Prompt photon production at large p_T in QCD beyond the leading order, Phys. Lett. **140B**, 87 (1984).

[2] J. F. Owens, Large momentum transfer production of direct photons, jets, and particles, Rev. Mod. Phys. **59**, 465 (1987).

[3] J. Huston, E. Kovacs, S. Kuhlmann, H. L. Lai, J. F. Owens, and W. K. Tung, Global QCD study of direct photon production, Phys. Rev. D **51**, 6139 (1995).

[4] P. Aurenche, M. Fontannaz, J. P. Guillet, B. A. Kniehl, E. Pilon, and M. Werlen, A critical phenomenological study of inclusive photon production in hadronic collisions, Eur. Phys. J. C **9**, 107 (1999).

[5] P. Aurenche, M. Fontannaz, J. P. Guillet, E. Pilon, and M. Werlen, Recent critical study of photon production in hadronic collisions, Phys. Rev. D **73**, 094007 (2006).

[6] P. Aurenche, R. Baier, M. Fontannaz, J. F. Owens, and M. Werlen, Gluon contents of the nucleon probed with real and virtual photons, Phys. Rev. D **39**, 3275 (1989).

[7] W. Vogelsang and A. Vogt, Constraints on the proton's gluon distribution from prompt photon production, Nucl. Phys. **B453**, 334 (1995).

[8] R. Ichou and D. d'Enterria, Sensitivity of isolated photon production at TeV hadron colliders to the gluon distribution in the proton, Phys. Rev. D **82**, 014015 (2010).

[9] D. d'Enterria and J. Rojo, Quantitative constraints on the gluon distribution function in the proton from collider isolated-photon data, Nucl. Phys. **B860**, 311 (2012).

[10] A. Aleedaneshvar, M. Goharipour, and S. Rostami, The uncertainty of parton distribution functions due to physical observables in a global analysis, Chin. Phys. C **41**, 023101 (2017).

[11] V. A. Bednyakov, M. A. Demichev, G. I. Lykasov, T. Stavreva, and M. Stockton, Searching for intrinsic charm in the proton at the LHC, Phys. Lett. B **728**, 602 (2014).

[12] S. Rostami, M. Goharipour, and A. Aleedaneshvar, Role of the intrinsic charm content of the nucleon from various light-cone models on $\gamma + c$-jet production, Chin. Phys. C **40**, 123104 (2016).

[13] J. Alam, S. Sarkar, P. Roy, T. Hatsuda, and B. Sinha, Thermal photons and lepton pairs from quark gluon plasma and hot hadronic matter, Ann. Phys. (N.Y.) **286**, 159 (2000).

[14] E. V. Shuryak, Quantum chromodynamics and the theory of superdense matter, Phys. Rep. **61**, 71 (1980).

[15] D. G. d'Enterria, Quark-gluon matter, J. Phys. G **34**, S53 (2007).

[16] M. M. Aggarwal *et al.* (WA98 Collaboration), Observation of Direct Photons in Central 158A GeV ^{208}P^{208}b + Pb Collisions, Phys. Rev. Lett. **85**, 3595 (2000).

[17] S. S. Adler *et al.* (PHENIX Collaboration), Centrality Dependence of Direct Photon Production in $\sqrt{s_{NN}} = 200$ GeV Au + Au Collisions, Phys. Rev. Lett. **94,** 232301 (2005).

[18] S. Afanasiev *et al.* (PHENIX Collaboration), Measurement of Direct Photons in Au + Au Collisions at $\sqrt{s_{NN}} = 200$ GeV, Phys. Rev. Lett. **109,** 152302 (2012).

[19] A. Adare *et al.* (PHENIX Collaboration), Enhanced Production of Direct Photons in Au + Au Collisions at $\sqrt{s_{NN}} = 200$ GeV and Implications for the Initial Temperature, Phys. Rev. Lett. **104,** 132301 (2010).

[20] A. Adare *et al.* (PHENIX Collaboration), Centrality dependence of low-momentum direct-photon production in Au + Au collisions at $\sqrt{s_{NN}} = 200$ GeV, Phys. Rev. C **91,** 064904 (2015).

[21] L. Adamczyk *et al.* (STAR Collaboration), Direct virtual photon production in Au + Au collisions at $\sqrt{s_{NN}} = 200$ GeV, arXiv:1607.01447.

[22] G. Aad *et al.* (ATLAS Collaboration), Centrality, rapidity and transverse momentum dependence of isolated prompt photon production in lead-lead collisions at $\sqrt{s_{NN}} = 2.76$ TeV measured with the ATLAS detector, Phys. Rev. C **93,** 034914 (2016).

[23] S. Chatrchyan *et al.* (CMS Collaboration), Measurement of isolated photon production in pp and PbPb collisions at $\sqrt{s_{NN}} = 2.76$ TeV, Phys. Lett. B **710,** 256 (2012).

[24] M. Wilde (ALICE Collaboration), Measurement of direct photons in pp and Pb-Pb collisions with ALICE, Nucl. Phys. **A904-905,** 573c (2013).

[25] J. Adam *et al.* (ALICE Collaboration), Direct photon production in Pb-Pb collisions at $\sqrt{s_{NN}} = 2.76$ TeV, Phys. Lett. B **754,** 235 (2016).

[26] A. Adare *et al.* (PHENIX Collaboration), Direct photon production in $d + $ Au collisions at $\sqrt{s_{NN}} = 200$ GeV, Phys. Rev. C **87,** 054907 (2013).

[27] T. Peitzmann (ALICE FoCal Collaboration), Measurement of forward direct photon production in p-A at the LHC with ALICE–A probe for nuclear PDFs and saturation, *Proc. Sci.*, DIS2016 (2016) 273.

[28] J. C. Collins, D. E. Soper, and G. F. Sterman, Factorization of hard processes in QCD, Adv. Ser. Dir. High Energy Phys. **5,** 1 (1989).

[29] R. Brock, J. Smith, J. C. Collins, J. Whitmore, R. Brock, J. Huston, J. Pumplin, W.-K. Tung, H. Weerts, C.-P. Yuan, S. Kuhlmann, S. Mishra, J. G. Morfín, F. Olness, J. Owens, J. Qiu, and D. E. Soper (CTEQ Collaboration), Handbook of perturbative QCD, Rev. Mod. Phys. **67,** 157 (1995).

[30] I. Schienbein, J. Y. Yu, K. Kovarik, C. Keppel, J. G. Morfin, F. Olness, and J. F. Owens, Parton distribution function nuclear corrections for charged lepton and neutrino deep inelastic scattering processes, Phys. Rev. D **80,** 094004 (2009).

[31] K. Kovařík, A. Kusina, T. Ježo, D. B. Clark, C. Keppel, F. Lyonnet, J. G. Morfín, F. I. Olness, J. F. Owens, I. Schienbein, and J. Y. Yu, nCTEQ15: Global analysis of nuclear parton distributions with uncertainties in the CTEQ framework, Phys. Rev. D **93,** 085037 (2016).

[32] K. J. Eskola, H. Paukkunen, and C. A. Salgado, EPS09–A new generation of NLO and LO nuclear parton distribution functions, J. High Energy Phys. 04 (2009) 065.

[33] D. de Florian, R. Sassot, P. Zurita, and M. Stratmann, Global analysis of nuclear parton distributions, Phys. Rev. D **85,** 074028 (2012).

[34] M. Hirai, S. Kumano, and T.-H. Nagai, Determination of nuclear parton distribution functions and their uncertainties in next-to-leading order, Phys. Rev. C **76,** 065207 (2007).

[35] H. Khanpour and S. Atashbar Tehrani, Global analysis of nuclear parton distribution functions and their uncertainties at next-to-next-to-leading order, Phys. Rev. D **93,** 014026 (2016).

[36] M. Hirai, Update of HKN nuclear PDFs, J. Phys. Soc. Jpn. Conf. Proc. **12,** 010024 (2016).

[37] K. J. Eskola, P. Paakkinen, H. Paukkunen, and C. A. Salgado, EPPS16: Nuclear parton distributions with LHC data, arXiv:1612.05741.

[38] R. Wang, X. Chen, and Q. Fu, Global study of nuclear modifications on parton distribution functions, arXiv: 1611.03670.

[39] F. Arleo and T. Gousset, Measuring gluon shadowing with prompt photons at RHIC and LHC, Phys. Lett. B **660,** 181 (2008).

[40] C. Brenner Mariotto and V. P. Goncalves, Nuclear shadowing and prompt photons in hadronic collisions at ultra-relativistic energies, Phys. Rev. C **78,** 037901 (2008).

[41] L. J. Zhou, H. Zhang, and E. Wang, Shadowing effects in direct photon and hadron production in heavy-ion collisions, J. Phys. G **37,** 105109 (2010).

[42] F. Arleo, K. J. Eskola, H. Paukkunen, and C. A. Salgado, Inclusive prompt photon production in nuclear collisions at RHIC and LHC, J. High Energy Phys. 04 (2011) 055.

[43] I. Helenius, K. J. Eskola, and H. Paukkunen, Probing the small-x nuclear gluon distributions with isolated photons at forward rapidities in $p + $ Pb collisions at the LHC, J. High Energy Phys. 09 (2014) 138.

[44] S. Alekhin, J. Blumlein, and S. Moch, The ABM parton distributions tuned to LHC data, Phys. Rev. D **89,** 054028 (2014).

[45] S. Dulat, T.-J. Hou, J. Gao, M. Guzzi, J. Huston, P. Nadolsky, J. Pumplin, C. Schmidt, D. Stump, and C.-P. Yuan, New parton distribution functions from a global analysis of quantum chromodynamics, Phys. Rev. D **93,** 033006 (2016).

[46] L. A. Harland-Lang, A. D. Martin, P. Motylinski, and R. S. Thorne, Parton distributions in the LHC era: MMHT 2014 PDFs, Eur. Phys. J. C **75,** 204 (2015).

[47] R. D. Ball, V. Bertone, S. Carrazza, C. S. Deans, L. Del Debbio, S. Forte, A. Guffanti, N. P. Hartland, J. I. Latorre, J. Rojo, and M. Ubiali (NNPDF Collaboration), Parton distributions for the LHC Run II, J. High Energy Phys. 04 (2015) 040.

[48] P. Jimenez-Delgado and E. Reya, Delineating parton distributions and the strong coupling, Phys. Rev. D **89,** 074049 (2014).

[49] H. Abramowicz *et al.* (H1 and ZEUS Collaborations), Combination of measurements of inclusive deep inelastic $e^{\pm}p$ scattering cross sections and QCD analysis of HERA data, Eur. Phys. J. C **75,** 580 (2015).

[50] A. Accardi, L. T. Brady, W. Melnitchouk, J. F. Owens, and N. Sato, Constraints on large-x parton distributions from new weak boson production and deep-inelastic scattering data, Phys. Rev. D **93,** 114017 (2016).

[51] J. Butterworth, S. Carrazza, A. Cooper-Sarkar, A. De Roeck, J. Feltesse, S. Forte, J. Gao, S. Glazov, J. Huston, Z. Kassabov, R. McNulty, A. Morsch, P. Nadolsky, V. Radescu, J. Rojo, and R. Thorne, PDF4LHC recommendations for LHC Run II, J. Phys. G **43,** 023001 (2016).

[52] A. D. Martin, R. G. Roberts, W. J. Stirling, and R. S. Thorne, Parton distributions: A New global analysis, Eur. Phys. J. C **4,** 463 (1998).

[53] D. Stump, J. Huston, J. Pumplin, W. K. Tung, H. L. Lai, S. Kuhlmann, and J. F. Owens, Inclusive jet production, parton distributions, and the search for new physics, J. High Energy Phys. 10 (2003) 046.

[54] P. Aurenche, R. Baier, M. Fontannaz, and D. Schiff, Prompt photon production at large p_T scheme invariant QCD predictions and comparison with experiment, Nucl. Phys. **B297,** 661 (1988).

[55] P. Aurenche, R. Baier, and M. Fontannaz, Prompt photon production at colliders, Phys. Rev. D **42,** 1440 (1990).

[56] H. Baer, J. Ohnemus, and J. F. Owens, Next-to-leading logarithm calculation of direct photon production, Phys. Rev. D **42,** 61 (1990).

[57] E. L. Berger and J. w. Qiu, Calculations of prompt photon production in QCD, Phys. Rev. D **44,** 2002 (1991).

[58] L. E. Gordon and W. Vogelsang, Polarized and unpolarized isolated prompt photon production beyond the leading order, Phys. Rev. D **50,** 1901 (1994).

[59] J. Cleymans, E. Quack, K. Redlich, and D. K. Srivastava, Prompt photon production in p-p collisions, Int. J. Mod. Phys. A **10,** 2941 (1995).

[60] G. P. Skoro, M. Zupan, and M. V. Tokarev, Asymmetry of prompt photon production in $\vec{p} - \vec{p}$ collisions at RHIC, Nuovo Cimento A **112,** 809 (1999).

[61] M. Fontannaz, J. P. Guillet, and G. Heinrich, Isolated prompt photon photoproduction at NLO, Eur. Phys. J. C **21,** 303 (2001).

[62] S. Catani, M. Fontannaz, J. P. Guillet, and E. Pilon, Cross section of isolated prompt photons in hadron hadron collisions, J. High Energy Phys. 05 (2002) 028.

[63] Z. Belghobsi, M. Fontannaz, J.-P. Guillet, G. Heinrich, E. Pilon, and M. Werlen, Photon-jet correlations and constraints on fragmentation functions, Phys. Rev. D **79,** 114024 (2009).

[64] P. Bolzoni, S. Forte, and G. Ridolfi, Renormalization group approach to Sudakov resummation in prompt photon production, Nucl. Phys. **B731,** 85 (2005).

[65] A. V. Lipatov and N. P. Zotov, Prompt photon hadroproduction at high energies in the k_T-factorization approach, J. Phys. G **34,** 219 (2007).

[66] I. Helenius, K. J. Eskola, and H. Paukkunen, Centrality dependence of inclusive prompt photon production in $d +$ Au, Au $+$ Au, $p +$ Pb, and Pb $+$ Pb collisions, J. High Energy Phys. 05 (2013) 030.

[67] S. Odaka and Y. Kurihara, Consistent simulation of direct-photon production in hadron collisions including associated two-jet production, Mod. Phys. Lett. A **31,** 1650099 (2016).

[68] M. D. Schwartz, Precision direct photon spectra at high energy and comparison to the 8 TeV ATLAS data, J. High Energy Phys. 09 (2016) 005.

[69] T. Jezo, M. Klasen, and F. Knig, Prompt photon production and photon-hadron jet correlations with POWHEG, J. High Energy Phys. 11 (2016) 033.

[70] A. V. Lipatov and M. A. Malyshev, Reconsideration of the inclusive prompt photon production at the LHC with k_T-factorization, Phys. Rev. D **94,** 034020 (2016).

[71] A. K. Kohara and C. Marquet, Prompt photon production in double-Pomeron-exchange events at the LHC, Phys. Lett. B **757,** 393 (2016).

[72] S. Benic, K. Fukushima, O. Garcia-Montero, and R. Venugopalan, Probing gluon saturation with next-to-leading order photon production at central rapidities in proton-nucleus collisions, J. High Energy Phys. 01 (2017) 115.

[73] F. Siegert, A practical guide to event generation for prompt photon production, arXiv:1611.07226.

[74] J. M. Campbell, R. K. Ellis, and C. Williams, Direct photon production at next-to-next-to-leading order, arXiv:1612.04333.

[75] S. Turbide, C. Gale, E. Frodermann, and U. Heinz, Electromagnetic radiation from nuclear collisions at RHIC energies, Phys. Rev. C **77,** 024909 (2008).

[76] I. Vitev and B. W. Zhang, A systematic study of direct photon production in heavy ion collisions, Phys. Lett. B **669,** 337 (2008).

[77] Z. Kunszt and Z. Trocsanyi, QCD corrections to photon production in association with hadrons in e^+e^- annihilation, Nucl. Phys. **B394,** 139 (1993).

[78] E. W. N. Glover and A. G. Morgan, Measuring the photon fragmentation function at LEP, Z. Phys. C **62,** 311 (1994).

[79] S. Frixione, Isolated photons in perturbative QCD, Phys. Lett. B **429,** 369 (1998).

[80] G. Aad et al. (ATLAS Collaboration), A measurement of the ratio of the production cross sections for W and Z bosons in association with jets with the ATLAS detector, Eur. Phys. J. C **74,** 3168 (2014); V. Khachatryan et al. (CMS Collaboration), Differential cross section measurements for the production of a W boson in association with jets in protonâ proton collisions at $\sqrt{s} = 7$ TeV, Phys. Lett. B **741,** 12 (2015).

[81] G. Aad et al. (ATLAS Collaboration), Measurement of the cross section for the production of a W boson in association with b^- jets in pp collisions at $\sqrt{s} = 7$ TeV with the ATLAS detector, Phys. Lett. B **707,** 418 (2012); Measurement of the production of a W boson in association with a charm quark in pp collisions at $\sqrt{s} = 7$ TeV with the ATLAS detector, J. High Energy Phys. 05 (2014) 068.

[82] G. Aad et al. (ATLAS Collaboration), Measurement of the production cross section of jets in association with a Z boson in pp collisions at $\sqrt{s} = 7$ TeV with the ATLAS detector, J. High Energy Phys. 07 (2013) 032; Measurement of differential production cross-sections for a Z boson in association with b-jets in 7 TeV proton-proton collisions with the ATLAS detector, J. High Energy Phys. 10 (2014) 141.

[83] V. Khachatryan et al. (CMS Collaboration), Measurement of the Isolated Prompt Photon Production Cross Section in pp Collisions at $\sqrt{s} = 7$ TeV, Phys. Rev. Lett. **106,** 082001 (2011); S. Chatrchyan et al. (CMS Collaboration), Measurement of the differential cross section for isolated prompt photon production in pp collisions at 7 TeV, Phys. Rev. D **84,** 052011 (2011).

[84] G. Aad et al. (ATLAS Collaboration), Measurement of the inclusive isolated prompt photon cross section in pp collisions at $\sqrt{s} = 7$ TeV with the ATLAS detector,

Phys. Rev. D **83**, 052005 (2011); Measurement of the inclusive isolated prompt photon cross-section in pp collisions at $\sqrt{s} = 7$ TeV using 35 pb^{-1} of ATLAS data, Phys. Lett. B **706**, 150 (2011).

[85] G. Aad *et al.* (ATLAS Collaboration), Measurement of the inclusive isolated prompt photons cross section in pp collisions at $\sqrt{s} = 7$ TeV with the ATLAS detector using 4.6 fb^{-1}, Phys. Rev. D **89**, 052004 (2014).

[86] G. Aad *et al.* (ATLAS Collaboration), Measurement of the inclusive isolated prompt photon cross section in pp collisions at $\sqrt{s} = 8$ TeV with the ATLAS detector, J. High Energy Phys. 08 (2016) 005.

[87] M. Aaboud *et al.* (ATLAS Collaboration), Measurement of the cross section for inclusive isolated-photon production in pp collisions at $\sqrt{s} = 13$ TeV using the ATLAS detector, arXiv:1701.06882.

[88] G. Aad *et al.* (ATLAS Collaboration), Measurement of the production cross section of an isolated photon associated with jets in proton-proton collisions at $\sqrt{s} = 7$ TeV with the ATLAS detector, Phys. Rev. D **85**, 092014 (2012).

[89] G. Aad *et al.* (ATLAS Collaboration), Dynamics of isolated-photon plus jet production in pp collisions at $\sqrt{s} = 7$ TeV with the ATLAS detector, Nucl. Phys. **B875**, 483 (2013).

[90] L. Bourhis, M. Fontannaz, and J. P. Guillet, Quarks and gluon fragmentation functions into photons, Eur. Phys. J. C **2**, 529 (1998).

[91] M. R. Whalley, D. Bourilkov, and R. C. Group, The Les Houches accord PDFs (LHAPDF) and Lhaglue, arXiv: hep-ph/0508110.

[92] R. Blair *et al.*, Report No. CERN-OPEN-2011-041, 2011, http://cds.cern.ch/record/1379880/files/CERN-OPEN-2011-041.pdf.

[93] M. L. Miller, K. Reygers, S. J. Sanders, and P. Steinberg, Glauber modeling in high energy nuclear collisions, Annu. Rev. Nucl. Part. Sci. **57**, 205 (2007).